Enhanced Methods Development for High-End Low-Fidelity Numerical Wing Weight and Flutter Prediction

António Carvalho de Paulo
antonio.paulo@tecnico.ulisboa.pt

Instituto Superior Técnico, Lisboa, Portugal

November 2015

Abstract

The work developed was based on an aeroelasticity tool created by Bauhaus Luftfahrt, named dAEDalus, and its objective was to improve the wing mass estimation. Therefore, two new modules were introduced: the first to include the high lift devices contribution into the dimensioning of the wing box; the second to predict the wing flutter speed. To estimate the mass of the devices were used several methods of different references, together with the ones here developed. The comparison between the devices' mass found with the different methods and the reference value of each aircraft, allowed to verify the estimates found. The implemented approach improved the initial wing mass estimate, fulfilling the proposed objective. The flutter speed was studied using an existing method, but corrected in such a way that allowed an improvement in its results. Verification was achieved by comparing the results with the Goland's wing. With this approach it was improved the speed estimate (more important parameter) in detriment of the frequency. Afterwards the method was implemented into dAEDalus to predict the flutter speed of some contemporary commercial aircraft wings. When the flutter speed was inside the minimum fail-safe clearance envelope, an optimization of the wing box was made to ensure the safety of the aircraft. The method allowed an estimation of the flutter speed of different aircraft, and the optimization loop made the wing flutter free inside the envelope. As the previous, this implementation also fulfilled the purposed objective.
Keywords: Aeroelasticity, dAEDalus, Flutter, Goland Wing, High Lift Devices

1. Introduction

The importance of having a tool that can predict with accuracy the size of a wing and respective wing box, is of major importance in the preliminary aircraft design field. There are a few methods capable of achieving a good precision in results, but their computational time is compromised. As such, it is relevant to find a tool that can achieve good precision with a low computational time.

This work aims for two fundamental accomplishments: the first one is to measure the influence of the high lift devices mass in the wing mass and in its box, as well as in the thickness of the wing box spars. The second one is to predict the flutter speed of a wing.

The basis of this document is an in-house aeroelastic tool named dAEDalus, that was developed at Bauhaus Luftfahrt. This tool couples a low-fidelity aerodynamic method, developed by (Melin, 2000), with a structure analysis method created primarily by (Seywald, 2011) and later improved by (Eisenbarth, 2013).

2. Theoretical Background

2.1. Aerodynamic Modeling

The aerodynamic model had to give a good prediction of the lift, induced drag and moment, since these are the most important in wing sizing. Also the model had to be computationally inexpensive, which means the computational time should not be excessive.

The aerodynamic forces and coefficients are calculated by a vortex lattice method called Tornado (Melin, 2000). Tornado is based on the method of (Moran, 1984) but was modified to accommodate a three dimensional solution and trailing edge control surfaces.

In Figure 1, the inputs and outputs of the aerodynamic module are specified. Here, a remark must be made to the deflections case, as they may or not be included as an input. As one may conclude from the analysis of the figure, this module is dependent of the geometry of the wing and the flight state and both are user requested inputs.

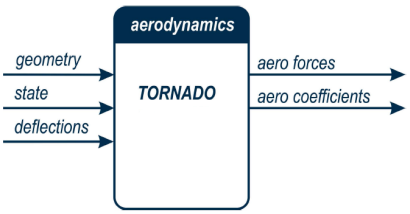

Figure 1: Aerodynamic module (Seywald, 2011)

2.2. Structural Modeling

Three dimensional non-linear finite elements were implemented to model the wing box. Each element has its own local coordinate system, that is later transformed to the global one using sweep, twist and dihedral angles. In Figure 2, the wing box positioning on the wing is depicted.

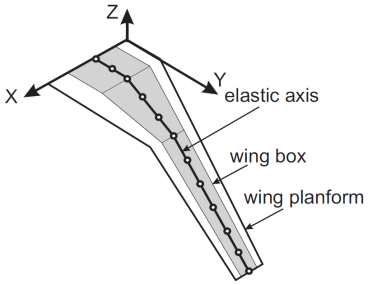

Figure 2: Wing box collocation on wing (Seywald, 2011)

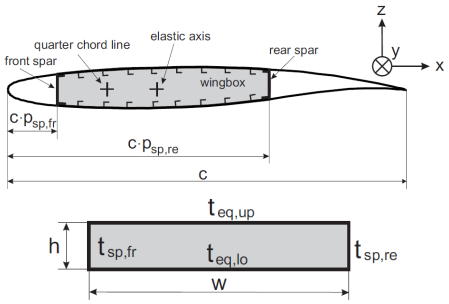

Figure 3: Wing box cross-section (Seywald, 2011)

The wing box is constituted by the spars, skin and stringers. The elastic axis, or shear center, is the point where a shear loads acts and produces zero twist. This is where the finite elements of the wing are positioned. A simplification of the wing box is made by concentrating the thickness of the skin and stringers into an equivalent one, so that it is possible to assume a rectangular shape. Also with this simplification, the thin-plate theory (Love, 1888) may be applied. This theory states that a mid-surface plane may be used to express a three dimensional plate in a two dimensional form. This process may be observed in Figure 3. The approximation used for the wing box was proven by (Bindolino et al., 2010) to be sufficient for the purpose of its usage.

2.3. Aerodynamic - Structural Coupling

In the case of dAEDalus, the mesh coupling was accomplished by converting the calculated displacements at the beam axis (corresponding to the elastic axis of the wing) to the two dimensional aerodynamic mesh. Hence a Dirichlet-Neumann coupling approach (Mehl et al., 2011) was used. In this method, the solution was found recurring to a staggered iteration procedure where, first, the aerodynamic (or fluid mesh) forces are determined and then they are related with the structural mesh. In order to transfer the information from the structural to the aerodynamic mesh, one has to use the estimated nodes displacements and then update them in the fluid mesh. This process is repeated until a convergence criteria is reached. Once the converged solution is found, a static equilibrium condition between the aerodynamic and the internal elastic restoring forces has been achieved.

2.4. Numerical Analysis Tool

The first procedure to occur in the script is the definition of the flight state conditions. Once this is done, the aerodynamic model is initiated to estimate the loads applied on the wing. Combining these loads with the external forces from the engines, landing-gear and high lift devices, a first calculation of the thickness of the structural components is made. As a result of the added thickness, the structural components now have a certain mass and stiffness, allowing to estimate the deformations suffered by the structural mesh. These deformations are transformed to the aerodynamic mesh and a second iteration of the loads takes place. The described process ends once a static converged solution is obtained. A final iteration is performed with the converged wing box mass to refine the wing mass.

To present an overview of the tool, the critical state loop is presented in Figure 4. In this overview, it is possible to identify each module: first are the aerodynamic and structural; then the combination of these two form the aeroelastic module (in Figure 4 the aeroelastic loop is referred as Structural Sizing Loop) and, at last, the critical state module contains all others.

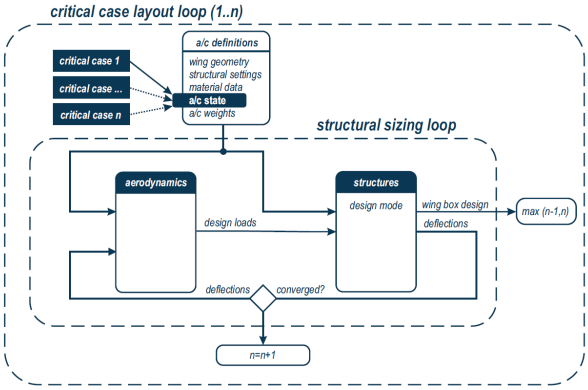

Figure 4: Critical state module (Seywald, 2011)

3. Implementation

3.1. High Lift Devices

As explained in (Rudolph, 1996), precise data on the masses of the HLD is not disclosed by the manufacturers. The data available results from studies performed by rival companies, therefore, a certain level of uncertainty is always attached to the mass prediction of such devices. This uncertainty can come from different places, for instance, the prediction made by two different engineering teams with different mentalities, one being more conservative and the other more progressive, or from changes in the concept and the type of technology used to produce the parts.

A diversified data basis was used to minimize the possible errors, such as the lack of information, and to do so different authors were studied (Roskam and Lan, 1997), (Paul, 1993), (Roskam, 1985), (Anderson et al., 1976), (Torenbeek, 1982) and (Torenbeek, 2013). Only the method developed from (Paul, 1993) is explained here, since the remaining methods are described by their authors.

An important remark must me made before the start of the next section. The aileron and spoiler are not high lift devices because the first induces a roll moment and the second acts as a speed break, but since they belong to the secondary structures of the wing, the available methods were used to predict their mass and to include them on the wing box sizing.

The following three methods were computed from (Paul, 1993). The **first mode** to estimate the HLD mass is created which relates the MTOW of the aircraft and the total mass of the HLD. The result is given by

$$m_1 = 8.996 \times 10^{-3} \cdot MTOW + 353.3\,. \qquad (1)$$

It is important to state that all the quantities are in [kg].

If the wing of the aircraft has more than one device, a correction has to be made to the value of the HLD mass, found with Equation (1). The adjustment accounts for the ratio between the area of the device and the total area of the HLD, resulting in

$$m_{HLD} = \frac{S_{HLD}}{S_{total}} m_{total}\,, \qquad (2)$$

where S_{total} is the total HLD area, $m_{total} = m_1$ is the total HLD mass and S_{HLD} is the area of the HLD, in [m^2].

The **second mode** uses the wing planform area to calculate the mass of all HLD and it is given by

$$m_2 = 6.782 \cdot S_{wing} + 124.116\,. \qquad (3)$$

It is interesting to note that this calculation mode does not have a dependency on MTOW (like the first mode), which can lead to larger errors when predicting the HLD total mass on two aircraft of the same family, that share the same wing geometry and, consequently, have the same area, as the Airbus A319, A320 and A321. As in the previous method, when the wing has more than one device, the total mass, m_2, is adjusted using Equation (2).

The **third mode** relates the MTOW and the mass of the devices located on the leading edge (LE) or the trailing edge (TE). Therefore, another two relations were created: the first computed the LE mass with the MTOW; the second estimated the TE mass, also, as a function of the MTOW of the aircraft. They are given by

$$m_{3_{le}} = 3.4374 \times 10^{-3} \cdot S_{HLD} + 134.24\,, \qquad (4)$$

$$m_{3_{te}} = 4.9403 \times 10^{-3} \cdot S_{HLD} + 346.33\,. \qquad (5)$$

In these relations, a worse correlation between these two quantities was obtained (as proved by the R-squared value), which may be related with the large sample of aircraft used, or with the fact that the MTOW in not a design criteria on the HLD mass prediction. Again, the procedure defined in Equation (2) is applied, when there is more than one device in the TE (or LE), to find the mass of a single device.

3.2. Flutter Prediction

3.2.1. Flutter Prediction Function

In the present case, it was assumed that the flutter motion of the wing can be represented by a combination of two fundamental uncoupled modes in bending and torsion. As the Goland wing has a uniform mass and stiffness distribution, these modes become the fundamental bending and torsion modes of an uniform beam. Therefore, the equations of motion are given by

$$L = m\ddot{w}_t \int f^2 \mathrm{d}y + m(x_f - x_{cg})\,\ddot{\theta}_t \int f\phi \mathrm{d}y + K_w\, w_t\,, \qquad (6)$$

$$\begin{aligned} M &= m(x_f - x_{cg})\ddot{w}_t \int f\phi \mathrm{d}y \qquad (7)\\ &\quad + (I_{cg} + m(x_f - x_{cg})^2)\,\ddot{\theta}_t \int \phi^2 \mathrm{d}y + K_\theta\,\theta_t\,, \end{aligned}$$

where y is the coordinate along the wingspan and the spring stiffnesses constants K_w and K_θ are defined by

$$K_w = EI \int \left(\frac{\mathrm{d}^2 f}{\mathrm{d}y^2}\right)^2 \mathrm{d}y\,, \qquad (8)$$

$$K_\theta = GJ \int \left(\frac{\mathrm{d}\phi}{\mathrm{d}y}\right)^2 \mathrm{d}y\,, \qquad (9)$$

where EI and GJ are the flexural and torsional rigidity, respectively, given in [$\mathrm{N} \cdot \mathrm{m}^2$].

An unsteady method is used to compute the lift and moment because it is able to predict with much

better accuracy the flutter phenomenon. The unsteady method takes into account the circulatory effects of lift, where the influence of the wake and the history of the flow are integrated. These terms contain the main damping and stiffness components.

In the present case, the Theodorsen's unsteady theory (Theodorsen, 1934) was used. This method introduced the Theodorsen transfer function, *C(k)*, that accounted for the attenuation of the lift amplitude and the phase lag due to the sinusoidal motion of the lift response. The Theodorsen transfer function incorporated a Padé approximation (that is used to develop a reduce order model of the airfoil, as in (Brunton and Rowley, 2011)).

The conversion of the transfer function into state space, requires the introduction of a new variable to close the system. It is called state space variable, u and is given by

$$\begin{aligned}\ddot{u} &= -\frac{0.3414}{a}\dot{u} - \frac{0.01582}{a^2}u + B_L V\theta_t \int f\phi \mathrm{d}y + \\ & B_L\left(\frac{c}{4}(1-2\hat{a})\right)\dot{\theta}_t \int f\phi \mathrm{d}y - B_L\dot{w}_t \int f^2 \mathrm{d}y \\ & . \end{aligned} \tag{10}$$

The total unsteady lift, L, in [N], and pitching moment, M, in [N · m], become

$$\begin{aligned}L &= -A_L\ddot{w}_t \int f^2\mathrm{d}y - A_L\frac{c}{2}\hat{a}\ddot{\theta}_t \int f\phi \mathrm{d}y \\ & -0.5176B_L\dot{w}_t \int f^2\mathrm{d}y + \frac{0.09845}{a}\dot{u} \\ & +\left(A_L V + 0.5176B_L\frac{c}{2}\right)\dot{\theta}_t \int f\phi\mathrm{d}y \\ & +0.5176B_L V\theta_t \int f\phi\mathrm{d}y + \frac{0.0075699}{a^2}u\,, \end{aligned} \tag{11}$$

$$M = Le + M_0\,, \tag{12}$$

$$\begin{aligned}M_0 &= A_L c\left[\frac{\ddot{w}_t}{2}\int f\phi\mathrm{d}y - \frac{c}{4}\left(\frac{1}{4}-\hat{a}\right)\ddot{\theta}_t\int\phi^2\mathrm{d}y \right. \\ & \left. -V\dot{\theta}_t\int\phi^2\mathrm{d}y\right]\,, \end{aligned} \tag{13}$$

where M_0 is the pitching moment at the aerodynamic center, ρ is the air density in [kg/m^3], C_{L_α} is the lift curve slope in [1/rad], V is the airspeed in [m/s] and c is the wing chord in [m], which constitute the constants $A_L = \frac{1}{2}\rho C_{L_\alpha}\frac{c^2}{4}$ and $B_L = \rho C_{L_\alpha} V\frac{c}{2}$.

3.2.2. State-Space Representation

Once the equations of motion are computed, the system takes a so called state-space representation. In this manner, the equations of motion are arranged into the following form

$$\begin{aligned}\{0\} &= \left([\underline{M}]-[\underline{A}]\right)\{\ddot{q}\} + \left([\underline{C}]-[\underline{B}]\right)\{\dot{q}\} \\ & +\left([\underline{K}]-[\underline{D}]\right)\{q\}\,, \end{aligned} \tag{14}$$

where $[\underline{M}]$ is the structural mass matrix, $[\underline{A}]$ is the aerodynamic mass matrix, $[\underline{C}]$ is the structural damping matrix, $[\underline{B}]$ is the aerodynamic damping matrix, $[\underline{K}]$ is the structural stiffness matrix and $[\underline{D}]$ is the aerodynamic stiffness matrix.

The state-space variable vector, $\{\underline{q}\}$, is defined as: $\{\underline{q}\} \equiv \{\underline{w}\,\theta\,u\}^\top$. Re-arranging Equation 14 one reaches the matrix system $[\underline{Q}]$, which is described by

$$[\underline{Q}] = \begin{bmatrix} [0] \\ -\left([\underline{M}]-[\underline{A}]\right)^{-1}\left([\underline{K}]-[\underline{D}]\right) \\ [\underline{I}] \\ -\left([\underline{M}]-[\underline{A}]\right)^{-1}\left([\underline{C}]-[\underline{B}]\right) \end{bmatrix}, \tag{15}$$

where $[\underline{I}]$ is the identity matrix and [0] is a null matrix, constituted by zeros.

The eigenvalues of the solution are computed from matrix $[\underline{Q}]$, making it possible to find the flutter speed and frequency. When two consecutive real parts of the eigenvalues have a different sign, and the imaginary part is not null, the flutter speed is found. If the imaginary part of the eigenvalue is null, then the result is not a flutter speed solution, but a divergence speed solution. On the other hand, the imaginary part of the eigenvalue is equivalent to the flutter frequency.

4. Results and Discussion

4.1. High Lift Devices

In this section, the results of the developed implementation are analyzed. A study of the final mass variation of the wing with the presence or absence of the HLD. A comparison is made between the original value (meaning before the inclusion of the HLD module into dAEDalus) and the new value (calculated with the enhanced version of dAEDalus) of the wing mass depending on the HLD mass prediction method used. The masses of the HLD calculated with the mass estimation methods are compared with (Paul, 1993). Despite being an old reference, it was not found another document that discretized the masses of the devices in different wings.

4.1.1. Airbus A320-200

In (Ajaj et al., 2013), a value for the A320--200 secondary systems weight is given, $WingSystemsEstimate = 0.30$, which means that 30% of the total wing structure mass is composed by the secondary systems. The *fueled_span* factor corresponds to the percentage of wingspan influenced by the fuel, and the value used was $fueled\_span = 0.50$, which was maintained from the previous dAEDalus version in (Eisenbarth, 2013).

The results of Table 1 show that, independently of the selected HLD mass prediction method, the

		Wing mass [kg]	**Error**	**HLD mass** [kg]	**Error**
Ref. (Paul, 1993)		9150	-	759.00	-
Without HLD		8588	-6.14%	-	-
HLD mass method	1	8286	-9.45%	1045.95	37.81%
	2	8312	-9.15%	958.54	26.29%
	3	8261	-9.71%	1125.65	48.31%
	4	8446	-7.69%	510.20	-32.78%
	5	8413	-8.05%	601.71	-20.72%
	6	8454	-7.61%	482.34	-36.45%
	7	8376	-8.45%	630.80	-16.89%

Table 1: A320-200 wing mass variation with HLD mass prediction method

final wing mass estimate is worse than the original value. From the previous results, the following trend is observed: when the HLD are heavier, the wing is lighter. This happens due to inertial relief exerted by the HLD and the greater they are, the larger the relief is and, consequently, the lighter the wing ends.

The seventh HLD mass prediction method is the one that yields the smallest error, but, on the other hand, the wing mass error is one of the largest. Nonetheless, the results make sense because with a larger inertia relief (due to the presence of the HLD) the final wing mass is lighter than the original.

The large errors found in the HLD column can arise from the made assumptions on the mass prediction methods, for instance:

- The baseline technology of the methods is too outdated, as for instance, the usage of aluminum as the predefined material since nowadays composites are usually employed in aircraft structures;
- The level of approximation used to define the HLD geometry on the wing and to calculate its characteristics, such as the area and the root and tip chords.
- The real values from (Paul, 1993) can include the actuators while the methods based on books or reports (fourth to the seventh) do not;
- The reference values retrieved from (Paul, 1993) are outdated, because of the fast evolution of the aircraft structures field;
- The first three methods are based on an equation supported by a small aircraft sample, which could lead to a good prediction of the HLD mass for certain aircraft and a bad one for others.

4.1.2. Parametric study of *WingSystemsEstimate* vs *fueled_span*

Since the A320 results with the inclusion of the HLD implementation showed an increase in the deviation (between the real wing mass value and the predicted one), a parametric study was conducted to evaluate the possibility of improving the wing and wing box mass. This was achieved by modifying two factors, the *WingSystemsEstimate* and *fuel_span* because they have an important influence in the final wing and wing box mass. In Figure 5, the relation between the three variables is given.

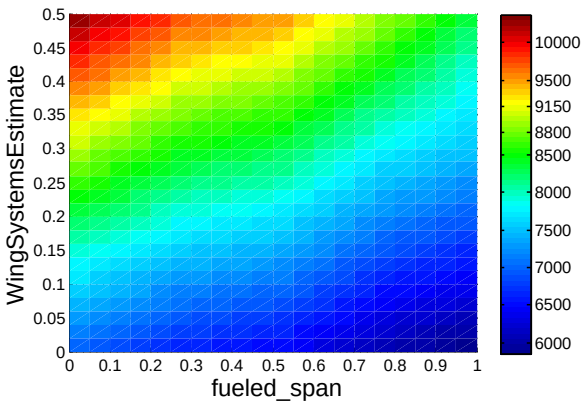

Figure 5: Wing mass [kg] vs *WingSystemsEstimate* vs *fueled_span* - xy plane

The region colored with yellow, as given in the color bar, represents the area where the results are closer to the reference wing mass value, that is $m_{wing} = 9150$[kg]. The red area expresses the values over the reference value. A clear evolution of the wing mass is retrieved from Figure 5, as explained below:

- *WingSystemsEstimate* - the increase of this factor also increases the wing mass. As it represents the mass of secondary systems in the wing, it makes sense that with an addition of these systems, the final wing mass increases;
- *fueled_span* - with fuel, the inertia relief of the wing increases, which helps balancing the loads applied on the wing. An increase in the

	Real	w/HLD	Combinations	
WingSystems Estimate	-	0.30	0.30	**0.40**
fueled_span	-	0.50	0.20	**0.33**
Wing mass [kg]	9150	8376	8625	**9165**
Error	-	-8.45%	-5.74%	**0.16%**

Table 2: A320-200 wing mass variation with *WingSystemsEstimate* and *fueled_span*

wingspan influenced with fuel leads to a lighter wing.

Table 2 contains the sequence of factors that produce the best wing mass estimate. Column one of this table includes the reference values of the wing, which was retrieved from (Paul, 1993).

By observing Table 2, it is possible to conclude that the two factors have a strong influence on the final mass of the wing. The last column of the computed combinations, in bold, indicates the best prediction of the wing mass. This way, the next set of factors produce the best estimate: $WingSystemsEstimate_{final} = 0.40$ and $fueled\_span_{final} = 0.33$, which are significantly different than the first set of values: $WingSystemsEstimate_{initial} = 0.30$ and $fueled\_span_{initial} = 0.50$.

With this combination the new wing mass of the Airbus A320-200 is $wing\_mass = 9165$ [kg], thus approaching the real value shown in Table 2.

4.2. Flutter

The goal is to find if the aircraft is fluttering or diverging inside its flight envelope. If outside of that region, the aircraft is declared safe and, in case the opposite is verified, the aircraft is subjected to an optimization loop, to transform its properties and make it flutter free.

4.2.1. Parametric Study of Flutter Speed and Frequency

In this section, a sensitivity study on the behavior of the flutter speed on Goland wing structural properties was conducted. The study was made by changing one property and keeping the others untouched. The range of the analysis started at -25% of its original value, up to +25%, in other words, $-25\%\, x_0 \leq x \leq +25\%\, x_0$. This range was chosen because it allowed to understand the behavior of the flutter speed, for a positive and a negative variation of the property in hand.

In the top plot of Figure 6, the results of the variables representing the deflections in Equations (6) and (8) are presented. The top plot includes the bending (that is related with the integral $\int f^2 \mathrm{d}y$), the torsion (with $\int \phi^2 \mathrm{d}y$) and the bending-torsion deflections (with $\int f\phi \mathrm{d}y$). The middle plot included the structural properties with the larger variation rate. At last, in the bottom plot were placed the remaining structural properties. In Figure 7, additional information on the variation of the flutter frequency with the properties is given.

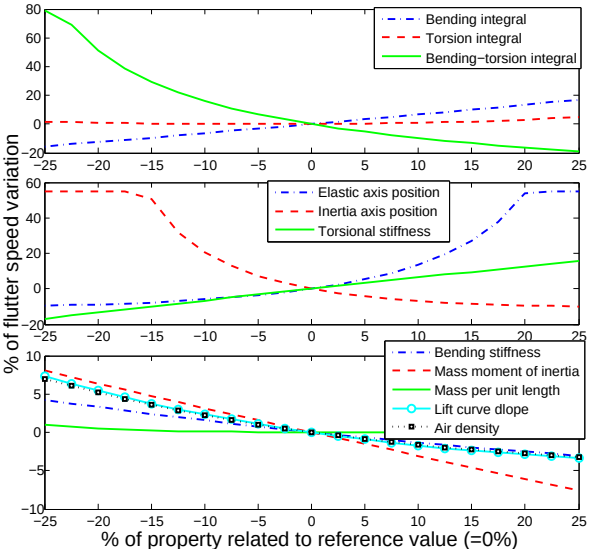

Figure 6: Flutter speed variation with selected properties

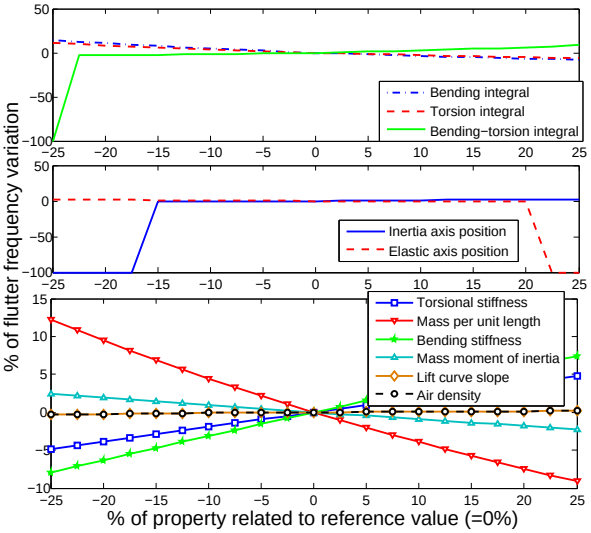

Figure 7: Flutter frequency variation with selected properties

The information presented in Figures 6 and 7 is used to justify the following conclusions:

- **Air density** - a heavier atmosphere tends to decrease the flutter speed since airplanes fly faster at higher altitudes, where the air pressure is smaller because there are fewer air molecules. Therefore, higher speeds have to be achieved, to destabilize the system;
- **Bending integral** - this property represents the bending deflections sustained by the wing and show an important influence in the flutter speed. Between the lower bound and the

upper bound, the flutter speed can change almost 40%. The importance of this parameter in the flutter frequency diminishes, since the variation drops to almost 20%;

- **Bending-torsion integral** - this parameter describes the coupling of the bending and torsion deflections and it shows that a smaller value tends to increase the flutter speed dramatically. Regarding the flutter frequency, as in the previous parameter, the variation observed is smaller than the flutter speed one. Nonetheless, for -25% of the reference value, a deviation on the frequency of -100% is registered, which means that the wing becomes divergence limited instead of flutter limited.
- **Bending stiffness** - an increased bending stiffness decreases the flutter speed because, for the same applied loads, the resulting wing deflections are smaller, which means that the necessary speed to destabilize the system decreases;
- **Elastic axis position** and **Inertia axis position** - unlike the other properties, the elastic axis position together with the inertia axis position have a nonlinear behavior since term (2,2) of matrix $[\underline{M}]$ is nonlinear. The variation observed in these properties is directly related with the distance between the two positions. As a design rule, to eliminate flutter it is good practice to coincide the elastic axis with the inertia axis of the wing because it eliminates the coupling between the bending and the torsional modes. The behavior found here proves this theory provided that: when the two positions are closer, the flutter speed increases; when they are farther apart, the flutter speed decreases. When the inertia axis position reaches $\approx$-17% and the elastic axis position $\approx$20%, the flutter frequency hits a plateau and instead of being flutter limited, the wing becomes divergence limited, as proven by the -100% variation in the mid plot of Figure 7.
- **Lift curve slope** - the behavior observed in the variation of this parameter is similar to the air density since a decrease in the lift curve slope, increases the flutter speed;
- **Mass per unit length** - the variation of the flutter speed with this property is almost negligible, because it stays very close to zero during the evaluation range, but the change of the flutter frequency is appreciable. A heavier wing tends to have a lower flutter frequency than a lighter one, which is comprehensible because with increased mass comes an increased inertia, making more difficult the up and down movement (frequency cycle) of the wing during its flight;
- **Mass moment of inertia** - Unlike the mass per unit length, this property shows a non negligible variation on the flutter speed. Frequency wise, it has a similar but attenuated behavior, sharing the same reasons with previous property;
- **Torsion integral** - this property represents the contribution of the torsion deflection in the model. It was observed a small increase in the flutter speed for the entire range of the study. In the flutter frequency, an increment was verified and virtually matched the values found in the bending deflection. Therefore, a variation in this parameter is almost only detected in the flutter frequency;
- **Torsional stiffness** - the change in this property leads to an important variation in the flutter speed and frequency. As the torsional stiffness increases, the warping angles suffered by the wing decrease, leading to a wing more resistant to the flutter phenomenon. The torsional stiffness is more important to the flutter speed variation than the bending stiffness and, when compared, the first almost makes the second negligible.

From the study conducted, it is possible to come up with a plan to modify the flutter speed. One way to increase the wing flutter speed is to decrease the distance between the elastic and the inertia axis (also referred to as mass balancing) and to increase the torsional stiffness of the wing. Mass balancing is one of the important concepts when dealing with flutter because a modification in the mass and stiffness distributions of the wing may lead to a significant increase in flutter speed. The increment of the torsional stiffness of the wing is done by increasing the torsion rigidity of the wing, which is going to decrease the torsion deflection and the coupling of the bending-torsion deflection, resulting in a large increase in the flutter speed.

The analysis of the wing flutter speed variation is very complex since a change of one property induces a modification in another, as they are all connected. Nonetheless, the objective of this study, with its simplifications, was to have an overall better understanding of the behavior of the method variables, together with the identification of the most relevant properties and that was accomplished.

4.2.2. Bombardier CRJ 900 vs Saab 2000

An analysis was made on two short range regional aircraft: the Bombardier CRJ900 has the jet engine positioned on the fuselage, behind the wing; while the Saab 2000 has the turboprop engine on the wing.

The engine positioning on the aircraft has a fundamental role on the flutter speed. Without the

engine on the wing, the CRJ900 loses an important damping and inertia force on the structure because of the size of the engine. On the other hand, the Saab 2000 has one engine on each wing, which is a good design feature to help increase the flutter speed because it moves the center of gravity of the wing forward.

These aircraft share some geometric properties, as it is possible to observe in Table 3, such as the wingspan, the wing area and, consequently, the aspect ratio. A high aspect ratio wing tends to be more prone to flutter than a low one and, in the present case, both wings have a high aspect ratio, which constitutes a negative contribution to the aircraft flutter speed.

The bending stiffness of the CRJ900 wing is six times larger than the S2000's, leading to the first negative contribution to the flutter speed of the CRJ900. Following to the torsional stiffness, unlike the previous parameter, the S2000's wing is stiffer than the CRJ900, contributing again negatively to the CRJ900 flutter speed.

The higher mass moment of inertia, together with the larger mass per unit length and with the greater distance between the elastic and the inertia axis, constitute three important negative contributions to the CRJ900's flutter speed.

Summing all the contributions of the structural properties, the final prediction is that the flutter speed of the CRJ900 is going to be much smaller than the S2000's.

In terms of the flutter frequency, not all properties give the advantage to the S2000, since the response observed in Section 4.2.1 for the structural parameters was different than the one for the flutter speed. For instance, the torsional stiffness is larger in the S2000, which helps increasing the flutter frequency, but a smaller bending stiffness has the opposite effect. Also, the smaller mass per unit length and the mass moment of inertia have a positive influence in the S2000's flutter frequency, increasing it.

In Tables 4 and 5, the results found for the Bombardier CRJ900 and the Saab 2000 are presented, respectively.

Altitude [ft]	**1.2V$_D$** [kn]	**Flutter Speed** [kn]	**Flutter Frequency** [rad/s]
0	720	384.87	28.35
13666	686	456.79	27.96
27333	649	552.04	27.58
41000	625	697.82	27.19

Table 4: Flutter results - Bombardier CRJ900

The predictions made before were confirmed, as the S2000 has a higher flutter speed and frequency than the CRJ900. The magnitude of the results found for the S2000 do not have any physical meaning and the only retrievable conclusion is that the aircraft is completely flutter free in its flight envelope.

Altitude [ft]	**1.2V$_D$** [kn]	**Flutter Speed** [kn]	**Flutter Frequency** [rad/s]
0	522	1669.72	90.38
10333	503	1846.61	89.95
20666	484	2105.14	89.44
31000	463	2472.51	88.75

Table 5: Flutter results - Saab 2000

In Figure 8, the results of each aircraft are plotted against the dive speed calculated from dAEDalus and the respective VMO, which were retrieved from (Jane, 2000) in the Saab 2000 case and from (FlightRun, 2012) for the Bombardier CRJ 900.

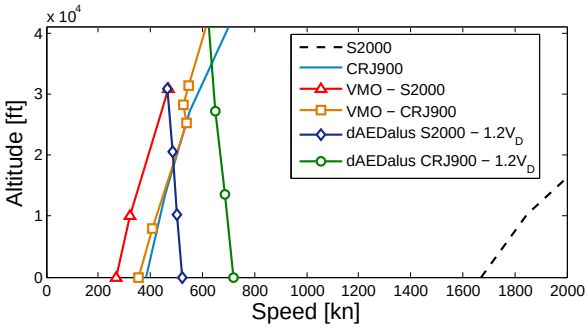

Figure 8: Flutter speed vs altitude - Bombardier CRJ900 and Saab 2000

It is observable in Figure 8, that the CRJ900 is flutter limited until ≈35000[ft], when the results cross the reference line set by the 1.2V$_D$ calculated with dAEDalus. In this way, the wing structure of this aircraft is subjected to the optimization loop, explained in Section **??** and detailed in Section 4.2.3, to make flutter unbounded over the entire flight envelope. Also, it is interesting to note the proximity between the VMO line and the flutter results of the CRJ900, given that the max operating speed takes into account the appearance of some phenomena as flutter. Furthermore it is known that the CRJ900 is not flutter limited on the real world, which means that the reference (equal to $1.2V_D$) used to decide if the aircraft is safe or not, might not be well estimated. Regarding the S2000, it is clearly confirmed that the aircraft is not flutter bounded so, the optimization loop option is discarded.

Concluding this section, the differences found in the flutter speed and frequency results are remarkable between two aircraft belonging to the same class, that share some geometric properties. Even with every structural parameter of the same order of magnitude, the final flutter speed results showed a difference of one order of magnitude, which is very

Parameter	Description	CRJ900	S2000
Aspect ratio	-	10.473	10.542
Engine position	(wing=1, fuselage=0)	0	1
int_2_f	Bending integral	0.963	0.377
int_2_ϕ	Torsion integral	0.0104	0.009
int_f_ϕ	Bending-torsion integral	0.0970	0.0107
I_{cg}	Mass moment of inertia, in [kg · m]	8.880E2	3.154E2
K_θ	Torsional stiffness, in [N · m/rad]	1.284E4	3.549E4
Kw	Bending stiffness, in [N/m]	9.632E4	1.5532E4
m	Mass per unit length, in [kg/m]	129.221	84.458
Sweep	LE sweep angle, in [deg]	34.342	6.175
x_f	Elastic axis position, in [m]	1.062	0.998
x_{cg}	Inertia axis position, in [m]	2.315	1.177
Wingspan	in [m]	24.900	24.762
Wing area	in [m^2]	49.204	48.162
Wing loading	in [kg/m^2]	616.521	392.003

Table 3: Structural properties - Bombardier CRJ900 and Saab 2000

significant.

4.2.3. Optimization Loop - Bombardier CRJ 900

The starting point of the loop corresponded to the dimensions of the cross section properties of the last critical case (refer to (Seywald, 2011)), because these ensured that the modified structure was able to resist the loads of the previous critical cases. A comparison between the newly optimized structural properties of the wing and the original ones is made in Table 6.

The stiffness of the modified wing is higher, resulting in a more resistant structure to the flutter instability. The integrals also reflect the increase in the wing stiffness, as their values were reduced by three orders of magnitude.

Due to significant increase in the spar and skin thicknesses of the beam elements, as well as on the stringers thickness and height, the wing mass increased considerably. This gain in mass was also reflected in the mass moment of inertia of the wing, which increased one order of magnitude. The variation in the spar and skin thickness is given in Figure 9, while the variation in the stringers properties is presented in Figure 10.

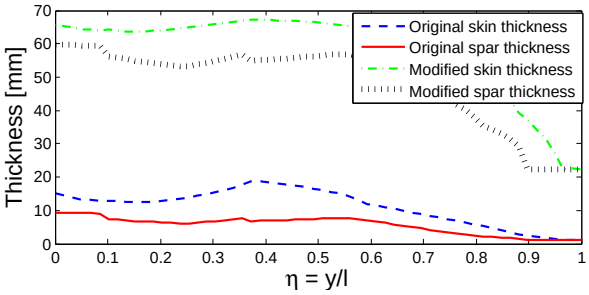

Figure 9: Spar and skin thickness variation with the flutter optimization loop

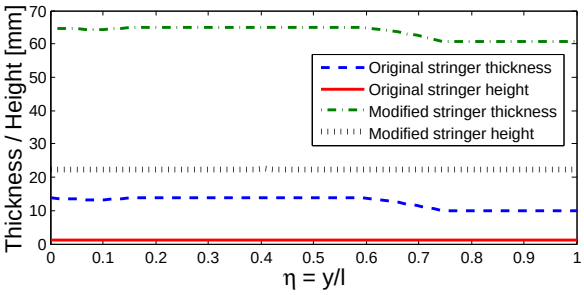

Figure 10: Stringers properties variation with the flutter optimization loop

As it is possible to observe in both figures, the dimensions of the properties increased dramatically. This is related with the low sensitivity of the solver to deal with the variation of these parameters. Despite the significant increase, all properties had distributions similar to the original ones, except the skin thickness that became smoother.

The results of the new optimized structure are presented in Table 7, where it is expected that the instability speed is over the barrier of the $1.2V_D$.

The expectations were met since the aircraft in now over the dive speed limit. In such a way that, it is believed the solver did a conservative estimation of the wing properties because the flutter speed is almost 300[kn] over the $1.2V_D$ limit. Together with the increase in speed, it was also verified a higher frequency, which is related with the gain in mass.

5. Conclusions

A method was fully developed to add the contribution of the HLD into the sizing of the wing box. It was verified using reference data from (Paul, 1993).

The flutter prediction function filled a gap in dAEDalus construction, and allowed the computation of the flutter speed and frequency of a wing. The optimization loop was able to solve the flutter

Parameter	Description	Original structure	New structure
int_2_f	Bending integral	0.963	0.007
int_2_ϕ	Torsion integral	0.0104	6.122E-5
int_f_ϕ	Bending-torsion integral	0.097	6.282E-5
I_{cg}	Mass moment of inertia, in [kg · m]	8.880E2	1.188E3
K_θ	Torsional stiffness, in [N · m/rad]	1.284E4	480.04
Kw	Bending stiffness, in [N/m]	9.632E4	3.6539E4
m	Mass per unit length, in [kg/m]	129.22	664.21
x_f	Elastic axis position, in [m]	1.062	1.087
x_{cg}	Inertia axis position, in [m]	2.315	2.445
Wing mass	in [kg]	3.218E3	1.654E4

Table 6: Modified structural properties - Bombardier CRJ900

		Original structure Flutter		Optimized structure Flutter	
Altitude [ft]	**1.2V$_D$** [kn]	**Speed** [kn]	**Frequency** [rad/s]	**Speed** [kn]	**Frequency** [rad/s]
0	720	384.87	28.35	1012.72	32.67
13666	686	456.79	27.96	1211.09	31.70
27333	649	552.04	27.58	1477.28	30.86
41000	625	697.82	27.19	1879.65	30.07

Table 7: Optimization results - Bombardier CRJ900

problem of a wing, by simply modifying the wing box cross section.

Despite the inclusion of the new implementations, the computational time of dAEDalus was kept small, except when the user chooses to use the optimization loop.

References

Ajaj, R., Smith, D., and Isikveren, A. (2013). A conceptual wing box weight estimation model for transport aircraft. *Aeronautical Journal*, 177(1191):533–551.

Anderson, R., Flora, C., Nelson, M., Raymond, E., and Vincent, J. (1976). Development of weight and cost estimates for lifting surfaces with active controls. Technical report, NASA.

Bindolino, G., Ghiringhelli, G., Ricci, S., and Terraneo, M. (2010). Multilevel structure optimization for preliminary wing box weight estimation. *Journal of Aircraft*.

Brunton, S. and Rowley, C. (2011). Low-dimensional state-space representations for classical unsteady aerodynamic models. *American Institute of Aeronautics and Astronautics*, (476). DOI: 10.2514/6.2011-476.

Eisenbarth, D. (2013). Elastic instability analysis and integration for a non-linear structural design tool. Master's thesis, Institute of Aircraft Design - Technische Universität München, Munich, Germany.

FlightRun (2012). Bombardier CRJ900 Performance. Sun Airlines Team. `http://www.flightrun.com/bombardier-crj900/performance`. Extracted on 4th August 2015.

Jane, F. (2000). *Jane's All the World's Aircraft*. Jane's Information Group. ISBN: 9780710620118.

Love, A. E. H. (1888). On the small free vibrations and deformations of elastic shells. *Philosophical trans. of the Royal Society*, series A(17):491–549. London.

Mehl, M., Janos, B., and Bungartz, H. J. (2011). Challenges and solution approaches for partitioned multi physics simulations. Technische Universität München, Munich, Germany, `http://www5.in.tum.de/pub/mehl_MunichMultiphysics2011.pdf`.

Melin, T. (2000). A vortex lattice MATLAB® implementation for linear aerodynamic wing applications. Master's thesis, Royal Institute of Technology, Stockholm, Sweden.

Moran, J. (1984). *Computational Fluid Dynamics*. John Wiley and Sons.

Paul (1993). Flügel transporter masserelevante daten. Technical Report 501 52-01, LTH Masseanalyse - Deutsche Aerospace Airbus. Hamburg, Germany.

Roskam, J. (1985). *Airplane Design: Preliminary configuration design and integration of the propulsion system*. Airplane Design. DARcorporation. ISBN: 9781884885433.

Roskam, J. and Lan, C.-T. (1997). *Airplane Aerodynamics and Performance*. DARcorporation. ISBN: 9781884885440.

Rudolph, P. (1996). High lift systems on commercial subsonic airliners. Technical Report 4746, NASA.

Seywald, K. (2011). Wingbox mass prediction considering quasi-static nonlinear aeroelasticity. Master's thesis, Royal Institute of Technology, Stockholm, Sweden.

Theodorsen, T. (1934). General theory of aerodynamic instability and the mechanism of flutter. Technical Report 496, National Advisory Committee for Aeronautics, Langley Field, Virginia, USA.

Torenbeek, E. (1982). *Synthesis of Subsonic Airplane Design*. Kluwer Academic Publishers. ISBN: 9024727243.

Torenbeek, E. (2013). *Advanced Aircraf Design - Conceptual Design, Analysis and Optimization of Subsonic Civil Airplanes*. John Wiley and Sons. ISBN:9781118568118.